THE JOURNAL OF BIOLOGICAL CHEMISTRY VOL. 288, NO. 10, pp. 7327–7337, March 8, 2013
© 2013 by The American Society for Biochemistry and Molecular Biology, Inc. Published in the U.S.A.

Expanding the Repertoire of Amyloid Polymorphs by Co-polymerization of Related Protein Precursors*

Received for publication, December 20, 2012, and in revised form, January 17, 2013 Published, JBC Papers in Press, January 17, 2013, DOI 10.1074/jbc.M112.447524

Claire J. Sarell[‡], Lucy A. Woods[‡], Yongchao Su[§], Galia T. Debelouchina[¶], Alison E. Ashcroft[‡], Robert G. Griffin[§], Peter G. Stockley[‡], and Sheena E. Radford[‡1]

From the [‡]Astbury Centre for Structural Molecular Biology and School of Molecular and Cellular Biology, University of Leeds, Leeds LS2 9JT, United Kingdom, the [§]Department of Chemistry and Francis Bitter Magnet Laboratory, Massachusetts Institute of Technology, Cambridge, Massachusetts 02139, and the [¶]Department of Chemistry, Princeton University, Princeton, New Jersey 08544

Background: Amyloid fibrils *in vivo* are rarely composed of a single protein, yet the consequences of co-polymerization of different proteins are relatively poorly understood.
Results: Fibrils formed by co-polymerizing two variants of β_2-microglobulin were characterized alongside their homopolymer equivalents.
Conclusion: The three fibril types have different structural and thermodynamic properties.
Significance: Co-polymerization of protein precursors enhances the structural and thermodynamic diversity of amyloid fibrils.

Amyloid fibrils can be generated from proteins with diverse sequences and folds. Although amyloid fibrils assembled *in vitro* commonly involve a single protein precursor, fibrils formed *in vivo* can contain more than one protein sequence. How fibril structure and stability differ in fibrils composed of single proteins (homopolymeric fibrils) from those generated by co-polymerization of more than one protein sequence (heteropolymeric fibrils) is poorly understood. Here we compare the structure and stability of homo and heteropolymeric fibrils formed from human β_2-microglobulin and its truncated variant ΔN6. We use an array of approaches (limited proteolysis, magic angle spinning NMR, Fourier transform infrared spectroscopy, and fluorescence) combined with measurements of thermodynamic stability to characterize the different fibril types. The results reveal fibrils with different structural properties, different side-chain packing, and strikingly different stabilities. These findings demonstrate how co-polymerization of related precursor sequences can expand the repertoire of structural and thermodynamic polymorphism in amyloid fibrils to an extent that is greater than that obtained by polymerization of a single precursor alone.

Amyloid fibrils are formed by the self-assembly of natively unfolded proteins and peptides such as $A\beta_{40/42}$ in Alzheimer disease (1), α-synuclein in Parkinson disease (2), and islet amyloid polypeptide in type II diabetes mellitus (3). In addition, self-assembly of folded proteins with all-α, all-β, or mixed α/β structures are all involved in human amyloidosis. These classes of proteins include β_2-microglobulin (β_2m), the all-β precursor of fibrils in the disorders dialysis-related amyloidosis (4) and hereditary systemic amyloidosis (5).

Despite the different conformational properties of amyloidogenic precursors, the fibrils that they form share common structural characteristics: typically a long, straight, unbranched morphology and a cross-β architecture (6). Recent analyses of amyloid fibrils using MAS[2] NMR (7–10) and x-ray diffraction of crystals formed from short (4–7 residue) amyloidogenic peptides have revealed an array of structural architectures that conform to the cross-β fold (11). For some proteins/peptides the same amino acid sequence can form conformationally distinct amyloid structures by varying the growth conditions, revealing the polymorphism possible for an identical protein sequence (reviewed in Ref. 12). In other cases structural variations of the cross-β fold occur as metastable species during fibril assembly (9). Further complexity could arise by the conformational properties of the monomeric precursor (whether folded, partially folded, or disordered) influencing the fibril structure formed (13) or by the co-polymerization of related sequences into heteropolymeric fibrils (14–16).

The clinically important protein, human β_2-microglobulin ($h\beta_2m$), and its truncated variant, ΔN6, offer an opportunity to investigate the role of sequence and precursor conformation in amyloid polymorphism. $h\beta_2m$ is a 99-residue protein that has a seven β-stranded immunoglobulin fold (17). In the absence of additives such as Cu^{2+}, detergents, trifluoroethanol, lipids, collagen, or glycosaminoglycans, $h\beta_2m$ is not able to form amyloid fibrils *in vitro* at neutral pH (for review, see Ref. 18). Instead, the amyloid potential of $h\beta_2m$ is unfurled only by unfolding the

* This work was supported, in whole or in part, by National Institutes of Health Grants EB003151 and EB002026. This work was also supported by Medical Research Council Grant G0900958, the Wellcome Trust (grant code 075099/Z/04/Z (LCT Premier, mass spectrometry facility) and NMR (094232)), and the Biotechnology and Biological Sciences Research Council, Swindon, United Kingdom (BB/526502/1) (BB/E012558/I, for the Synapt HDMS).
⌘ *Author's Choice*—Final version full access.
[1] To whom correspondence should be addressed. Tel.: 44-113-34-33170; Fax: 44-113-34-37486; E-mail: s.e.radford@leeds.ac.uk.

[2] The abbreviations used are: MAS, magic angle spinning; $h\beta_2m$, human β_2-microglobulin; ANS, 8-anilino naphthalene sulfonate; HFIP, hexafluoroisopropanol; RFDR, radio frequency-driven recoupling; ZF TEDOR, Z-filtered transferred-echo double resonance; ThT, thioflavin T; TAMRA, 5(6)-carboxytetramethylrhodamine succinimidyl ester; GuHCl, guanidinium chloride; ESI, electrospray ionization.

protein, for example by acidification to pH 2 (19, 20). The fibrils formed under these conditions have been characterized in detail using MAS NMR (10), EPR (21), FTIR (22), limited proteolysis (23), and cryo-electron microscopy (EM) (24). These results have revealed that the fibrils formed from hβ_2m at pH 2 are composed of parallel, in-register β-strands that involve 90 of the 99 residues in the fibril core, the nine N-terminal residues retaining a dynamic conformation that is not integral to the fibril structure (10).

By contrast with the intransigence of hβ_2m to form amyloid-like fibrils at neutral pH, a natural variant of hβ_2m that is truncated by six residues at its N terminus (ΔN6) is able to form amyloid-like fibrils at pH 6–7 *in vitro* in the absence of additives (25). This truncation is the major modification of hβ_2m found in *ex vivo* fibrils (26). Despite truncation of the N-terminal six residues, ΔN6 displays only minor structural differences compared with hβ_2m in the native form (25). Although the structural properties of ΔN6 cannot explain its enhanced ability to form amyloid fibrils at neutral pH, increased conformational dynamics evidenced by NMR relaxation times (T_2 values) (25), hydrogen exchange protection (27–29), molecular dynamics simulations (30), and denaturation with guanidinium chloride (GuHCl) (31) have been linked to its ability to form fibrils at this pH.

In this study we examine how the amyloid fibrils formed from folded ΔN6 at pH 6.2 differ from those assembled by acid unfolded hβ_2m at pH 2. We characterize structural and thermodynamic differences between these two fibril types using MAS NMR, limited proteolysis with mass spectrometry, and spectroscopic measurements (FTIR, fluorescence, and ANS binding). Building on previous experiments which have shown that substoichiometric ratios of ΔN6 are able to convert hβ_2m into an amyloidogenic form at neutral pH (25), we examine how fibrils formed by co-incubation of these two proteins at pH 6.2 differ from those formed from each protein alone. The results reveal that the fibrils formed under each condition show different structural properties and side-chain packing and striking differences in their thermodynamic properties. The findings highlight the diversity of amyloid architectures that is possible for a given protein sequence and demonstrate how fibril polymorphism can be enhanced by the co-polymerization of proteins of related sequence.

EXPERIMENTAL PROCEDURES

Protein Preparation— hβ_2m and ΔN6 were produced as previously described (25). For NMR experiments ^{15}N and ^{13}C and ^{15}N-labeled ΔN6 was prepared as described in Ref. 10.

Solution NMR Spectroscopy—Samples of ^{15}N-labeled protein (1 mg/ml) in either 50 mM MES, 120 mM NaCl, pH 6.2, or 10 mM sodium phosphate buffer, 50 mM NaCl, pH 2, 90% (v/v) H_2O, 10% (v/v) D_2O were used for solution NMR experiments. Spectra were recorded at 25 °C on a Varian Inova 750 MHz spectrometer.

Assembly of Amyloid Fibrils—ΔN6 fibrils and the mixed fibril sample were assembled in 50 mM MES buffer, 120 mM NaCl at pH 6.2. The mixed fibril sample was formed from a 1:1 molar ratio of hβ_2m:ΔN6 monomers. hβ_2m fibrils were formed in 10 mM sodium phosphate buffer containing 50 mM NaCl, pH 2.0. Assembly usually began with 1 mg/ml soluble protein. Fibril growth was performed in a BMG Fluostar Optima plate reader at 37 °C at 600 rpm. A final concentration of 10 μM thioflavin T (ThT) was added where appropriate. Fibrils were left to assemble for ~5 days before analysis. Fibrillar hβ_2m for MAS NMR was formed at pH 2.5, as described in Ref. 10.

Detection of the Presence of an Intact Disulfide Bridge in ΔN6 Fibrils—ΔN6 fibrils (60 μl of 80 μM) were centrifuged at 14,000 × *g* for 20 min. The pellet was resuspended in hexafluoroisopropanol (HFIP), divided into three, and incubated overnight at 37 °C with gentle rotation (200 rpm), then air-dried. The first aliquot had no further treatment (control sample). 20 μl of 20 mM iodoacetamide in 50 mM ammonium bicarbonate, pH 7, was added to sample two (alkylated sample). This sample was then incubated in the dark at room temperature for 30 min. The third aliquot (reduced alkylated sample) was resuspended in 20 μl of 10 mM dithiothreitol in 50 mM ammonium bicarbonate, pH 7, and heated to 80 °C for 15 min. The sample was then cooled for 5 min at 4 °C and centrifuged at 14,000 × *g* for 20 min, and 20 μl of 20 mM iodoacetamide added to the supernatant. This sample was then incubated in the dark at room temperature for 30 min. Samples were analyzed by Z-spray nanoelectrospray ionization mass spectrometry.

MAS NMR— hβ_2m and ΔN6-hydrated fibrils (35 and 45 mg, respectively) were collected by centrifugation (265,000 × *g*) and packed into 3.2-mm Bruker zirconia rotors. Solid-state NMR experiments were conducted at 277 K on a Bruker 900 MHz spectrometer and a custom designed 750 MHz spectrometer (courtesy of Dr. David J. Ruben, Francis Bitter Magnet Laboratory, Cambridge, MA).

Two kinds of MAS NMR techniques, RFDR and ZF TEDOR, were utilized to establish one-bond ^{13}C-^{13}C and ^{13}C-^{15}N correlations, respectively (32–34). RFDR spectra were acquired at 20-kHz MAS on a 900-MHz spectrometer. The ^{13}C-^{13}C dipolar coupling was recoupled in the rotor-synchronized RFDR mixing period during which 12.5-μs π pulses and 83.3-kHz CW decoupling were applied on the ^{13}C and ^{1}H channels, respectively. A total RFDR mixing time of 1.6 ms was used to realize one-bond ^{13}C-^{13}C correlations. One-bond ZF TEDOR experiments were conducted on a 750-MHz spectrometer and under 12.5-kHz sample spinning, with a total dipolar recoupling time of 1.6 ms and ^{1}H TPPM decoupling at 95 kHz during mixing and 83 kHz during acquisition.

Fluorescent Labeling and Confocal Imaging of hβ_2m and ΔN6 Fibrils—A 10-fold molar excess of 5(6)-carboxytetramethylrhodamine succinimidyl ester (TAMRA) (Invitrogen) was titrated into monomeric hβ2m, and a 10-fold molar excess of fluorescein-5-isothiocyanate (FITC) (Molecular Probes) was titrated into monomeric ΔN6. Labeling was allowed to continue for 45 min. Fluorescently labeled monomers of each protein were then purified (PD10 desalting column), and fibrils were formed by mixing these samples as described above at a 1:10 molar ratio of fluorescently labeled protein to each unlabeled protein (34). Confocal images were captured on a DeltaVision Deconvolution Microscope. Colocalization analysis was performed using Image J. At each pixel location the contributing intensity from both channels was assessed, and a scatter graph was plotted.

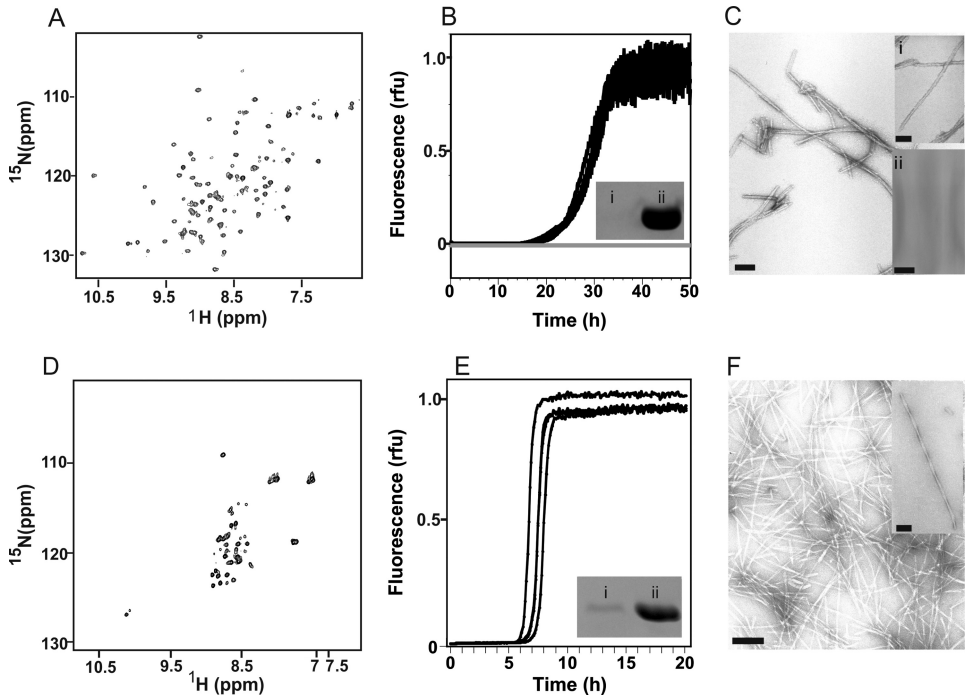

FIGURE 1. **Fibrils formed from hβ_2m and ΔN6.** *A*, shown is a ^{1}H,^{15}N HSQC spectrum of ΔN6 at pH 6.2. *B*, shown is fibril formation of 0.5 mg/ml ΔN6 (*black lines*) and hβ_2m (*gray lines*, no growth) at pH 6.2 measured using thioflavin T fluorescence (relative fluorescence units (*rfu*)). Three replicates for each protein are shown. The *inset* shows an SDS-polyacrylamide gel of the supernatant of the ΔN6 sample after an incubation time of 120 h (*lane i*) and before fibril growth (*lane ii*). *C*, shown are negative stain EM images of ΔN6 fibrils. *Inset i* shows an expanded view, and *inset ii* shows the absence of hβ_2m fibrils under the same conditions (*scale bar* = 100 nm). *D–F* are as in *A–C*, but for hβ_2m at pH 2.0 in 10 mM sodium phosphate, 50 mM sodium chloride.

Limited Proteolysis—Proteinases (chymotrypsin or aspergillopepsin I (Sigma)) were added at 1:100 (w/w) proteinase to protein ratios, and proteolysis was allowed to proceed for 30 min at 25 °C. Fibrillar samples were depolymerized after digestion in 100% (v/v) HFIP. Samples were air-dried then redissolved in 50:40:10 acetonitrile/water/acetic acid (v/v/v), and peptides were identified by infusing the sample into a Synapt HDMS (Micromass UK Ltd/Waters Corp., Manchester, UK) quadrupole-traveling wave IMS-oaTOF mass spectrometer.

Fourier Transform Infrared Spectroscopy—Monomeric proteins (2.5 mg/ml) were exchanged into D_2O. Fibrils were prepared as described above, except that the buffers were prepared using D_2O at the appropriate pD. Spectra were acquired on a Thermo-Nicolet 560 FTIR spectrometer.

Dot Blots—Dot blots using WO1 (35) and polyclonal anti-β_2m antibodies (Dako) were performed according to Xue *et al.* (36).

Intrinsic Fluorescence and 8-Anilino Naphthalene Fluorescence Measurements—The fluorescence of 2.5 μM monomer or fibrils was excited at 280 nm, and fluorescence emission was measured between 300 and 390 nm. The fluorescence of each sample was also measured in the presence of 250 μM ANS to 1 μM fibrils (monomer equivalent concentration). Excitation was at 389 nm. Fluorescence was measured using a Photon Technology International QM-1 spectrofluorimeter (PTI).

Determination of Fibril Stability—Fibrils (0.2 mg/ml) were diluted into different concentrations of GuHCl in the buffer in which each sample was prepared based on Shammas *et al.* (37). Solutions were incubated for 1.5 h at 25 °C then centrifuged in a Beckman ultracentrifuge at 313,000 × *g* for 45 min. The protein concentration of the supernatant was determined by the absorbance at 280 nm using an extinction coefficient of 20065 $cm^{-1}\,M^{-1}$ for both β_2m and ΔN6.

RESULTS

Homopolymeric Assembly of ΔN6 and Wild-type hβ_2m into Amyloid-like Fibrils—Previous experiments have shown that the kinetics of ΔN6 fibrillation depend critically on the solution pH, with an enhanced rate of fibril formation occurring as the pH is lowered from pH 8.2 to pH 6.2 (25). To form fibrils from ΔN6 under conditions in which the protein is initially folded but is able to assemble into amyloid-like fibrils rapidly, the conditions of fibril growth (pH, temperature, buffer ionic strength, and agitation rate) were varied. Here and throughout, ThT fluorescence was used to monitor the rate of fibril growth. Fibril yield and morphology were determined by estimation of the amount of unpolymerized monomer in the supernatants using SDS-PAGE and by negative stain transmission electron microscopy of the fibril samples. Having screened several different conditions, fibrils of ΔN6 were ultimately formed by incubation of 0.5 mg/ml protein in 50 mM MES, 120 mM NaCl (150 mM total ionic strength), pH 6.2, 37 °C, with agitation of 600 rpm in 96-well plates. Under these conditions ΔN6 is natively folded as judged by NMR (Fig. 1*A*), and fibrils form within 48 h with a yield of >98% (Fig. 1*B*, *black traces* and *inset*) without visible formation of amorphous aggregates (Fig. 1*C* and *inset i*).

By contrast with the rapid formation of amyloid-like fibrils by ΔN6 at pH 6.2, amyloid-like fibrils are not formed from native hβ_2m at pH 6.2, as judged by the same techniques (Fig. 1*B*, *solid gray line*, and *C*, *inset ii*). Acidification of hβ_2m to pH 2.0 results in a highly unfolded species (Fig. 1*D*) and renders the protein

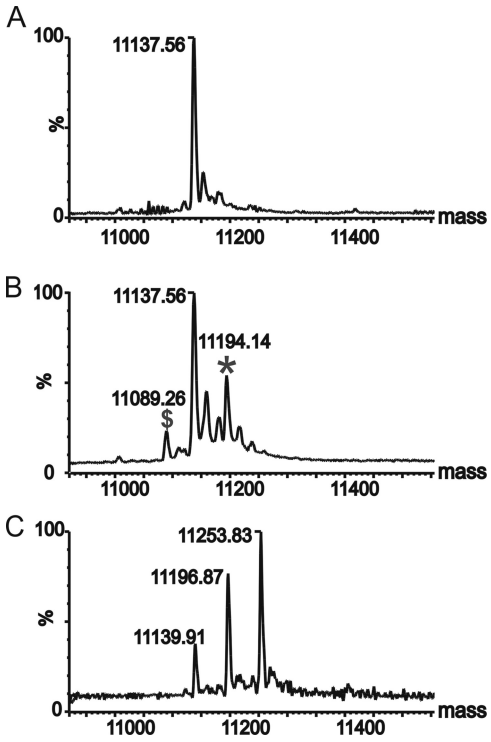

FIGURE 2. **ESI-MS spectra reveal that the disulfide bond is intact in ΔN6 fibrils.** *A*, shown are monomers of ΔN6 released from fibrils formed at pH 6.2 by treatment with HFIP. *B* is as *A*, but the sample was treated with a 20-fold molar excess of iodoacetamide. *, results from derivatization of methionine (11,194 Da) and a subsequent loss of the carboxyamido group (marked with $) (62). *C* is as *B*, but the sample was treated with DTT followed by the addition of a ~20-fold molar excess (over the total thiol concentration) of iodoacetamide.

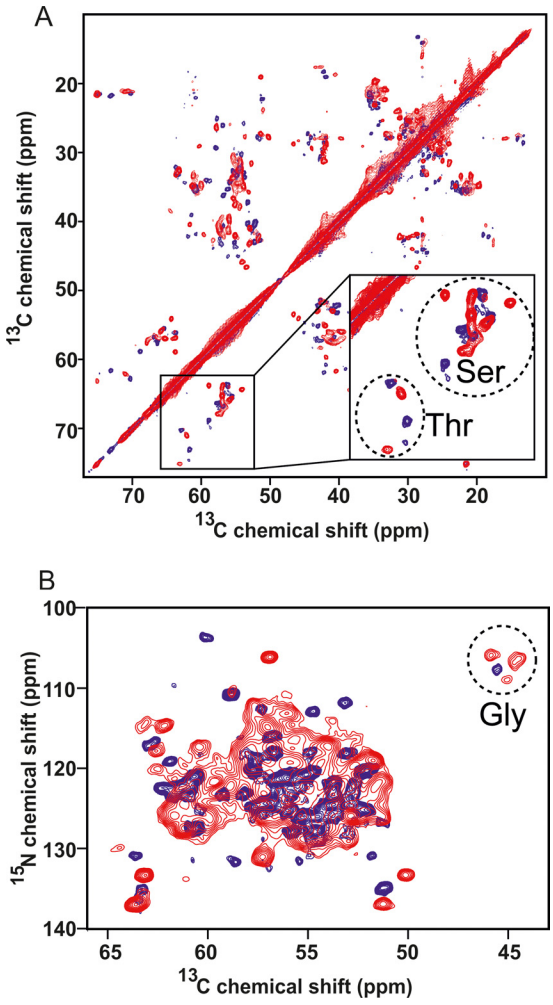

FIGURE 3. **MAS NMR spectra of uniformly ^{13}C,^{15}N-labeled hβ_2m (*blue*) and ΔN6 (*red*) fibrils.** *A*, shown are one-bond ^{13}C-^{13}C correlations from a RFDR experiment. *B*, shown are backbone Nα-Cα correlations obtained with ZF TEDOR.

readily able to form amyloid-like fibrils with ~90% yield (38) (Fig. 1, *E* and *F*).

Previous results have shown that reduction of the single disulfide bond in hβ_2m enhances its fibrillogenic potential and that disulfide bond interchange can initiate hβ_2m fibril formation (39). To determine whether the disulfide bond linking residues 25–80 in the ΔN6 monomer is intact in the fibrils formed from ΔN6 at pH 6.2, the fibrils were disassembled by incubation with HFIP, and the status of the disulfide bond was determined using chemical modification with iodoacetamide, monitored using ESI-MS ("Experimental Procedures"). The results of these experiments (Fig. 2) showed that monomers released from the ΔN6 fibrils in the absence or presence of iodoacetamide have a mass 11,137 ± 1.14 Da (Fig. 2, *A* and *B*), consistent with that expected for unmodified ΔN6 (11,137 Da). ΔN6 monomers released from fibrils treated with DTT and incubated with iodoacetamide resulted in a mixture of species (Fig. 2*C*): reduced, unalkylated protein (11,140 Da); alkylation of a single cysteine (11,196.9 Da); alkylation of both cysteines (11,253.8 Da). This demonstrates that the majority of monomers retain the disulfide linkage in the ΔN6 homopolymeric fibrils.

Structural Analysis of Fibrils Formed from ΔN6 and hβ_2m Using Solid State NMR—Our previous MAS NMR experiments have studied fibrils formed from hβ_2m at pH 2 (10). These studies identified a parallel-in-register intermolecular packing of the β-strands. The chemical shift analysis suggested that the β-strands within the fibril are distinct from those within native hβ_2m (25). Furthermore the MAS NMR experiments demonstrated that ~70% of the hβ_2m protein sequence participates in β-strands within the rigid fibril core of the full-length protein.

To determine whether the fibrils formed from ΔN6 and hβ_2m share structural homology at the residue-specific level, MAS NMR studies of the homopolymeric fibrils formed by ΔN6 at pH 6.2 were performed. Fig. 3*A* presents ^{13}C-^{13}C spectra of uniformly ^{13}C,^{15}N-labeled ΔN6 fibrils formed at pH 6.2 (red) and uniformly ^{13}C,^{15}N-labeled hβ_2m fibrils formed at pH 2.5 (blue). Fig. 3*B* shows the two-dimensional ^{15}N-^{13}C correlation spectra of each sample recorded with ZF TEDOR mixing of 1.6 ms, showing mostly backbone N-Cα correlations. The line width of cross-peaks in the ΔN6 spectra is 0.4–0.6 ppm for ^{13}C and 0.8–1.2 ppm for ^{15}N, comparable to peaks of hβ_2m fibrils in spectra acquired with the same acquisition parameters, suggesting similar structural homogeneity. No peak multiplicity was observed for either sample, with a single set of backbone ^{13}C and ^{15}N chemical shifts for all residues in these spectra, ruling out the possibility of polymorphism within each sample.

Compared with the spectra of hβ_2m fibrils, the spectra of ΔN6 fibrils contain more backbone Nα-Cα and Nα-CO cross-peaks for resolved amino acid types (Fig. 3*B*). For example,

three glycine cross-peaks were observed in spectra of the ΔN6 fibrils compared with only one glycine cross-peak in spectra of the hβ_2m fibrils (*circled* in Fig. 3*B*). These data suggest that ΔN6 fibrils are less dynamic than hβ_2m fibrils and hints that ΔN6 fibrils may possess a more extensive β-sheet core than their wild-type counterparts. Consistent with this, the MAS INEPT spectrum of ΔN6 fibrils contains only a few weak peaks (data not shown), suggesting that there are no regions that experience significant mobility in this truncated version of the protein. This is in contrast to fibrils formed from hβ_2m at pH 2.5 that showed significant dynamics for residues within the N-terminal 7 residues (10).

Further inspection of the spectra in Fig. 3 reveals that the majority of the cross-peaks are different and shifted from each other in the fibrils of ΔN6 and hβ_2m, suggesting distinct secondary structures. Some of the differences might arise from the difference in pH (6.2 *versus* 2.5), especially for sites that participate in hydrogen bonding, such as protonated side chains. However, such effects cannot explain the global changes observed in the chemical shifts. Taking the TEDOR spectrum for example (Fig. 3*B*), the three glycine residues in the ΔN6 spectrum (Gly-18, -29, and -43, *circled* in Fig. 3*B*) show clearly different chemical shifts to those of hβ_2m fibrils. Similarly, the differences in Ser and Thr Cα-Cβ correlations (*enlarged* and *circled* in Fig. 3*A*) are on the order of 2.5–4.0 ppm, too large to be attributed to the effect of pH alone (40). These observations suggest that there are significant differences in the molecular conformations of the proteins in the fibrils formed from hβ_2m and ΔN6. Further analysis, including residue-specific assignment, will be needed to define these differences in more detail.

Formation of Mixed ΔN6:hβ_2m Fibrils—Previous studies have shown that monomeric ΔN6 is able to convert hβ_2m into a conformation able to form amyloid fibrils at neutral pH. Quantitative incorporation of hβ_2m monomers into amyloid fibrils occurred when mixed with equimolar ΔN6 monomer at pH 6.2–7.2 (25). To further characterize the heteropolymeric fibrils formed by mixing monomeric hβ_2m and ΔN6, the two proteins were incubated separately or in an equimolar mixture at pH 6.2, and the formation of fibrils was monitored using ThT fluorescence (Fig. 4*A*). The results showed that hβ_2m alone is not able to form fibrils at pH 6.2 under the conditions employed (60 and 120 μM protein monomer, shown as *solid gray lines*), as confirmed by EM (Fig. 4*B*). In comparison, ΔN6 rapidly formed fibrils under these conditions (Fig. 4*A*, *black solid* and *dashed lines*). By contrast with previous results (25), under the conditions employed here, the rate of fibril growth decreases as the concentration of ΔN6 is increased from 60 μM to 120 μM, suggestive of a complex assembly reaction, involving the formation of off-pathway oligomers (Fig. 4*A*). Interestingly the mixed sample, which contained 60 μM concentrations of both ΔN6 and hβ_2m monomers, formed fibrils at a rate similar to that of 120 μM ΔN6 alone (Fig. 4*A*, *gray dotted lines*), consistent with co-polymerization of ΔN6 and hβ_2m during fibril assembly. The kinetics of fibril formation monitored using ThT fluorescence suggest that co-polymerization of hβ_2m and ΔN6 does not arise from ΔN6 seeding hβ_2m, as this would result in a lag phase similar (~20 h), if not shorter, than that of 60 μM ΔN6 incubated alone. Instead, fibril formation is not observed in the mixed sample until ~40 h of incubation. Transmission electron microscopy of the fibrils formed in the mixed sample (Fig. 4*C* and *inset*) confirmed the presence of fibrils, which have a long straight unbranched morphology.

To determine whether co-incubation of hβ_2m and ΔN6 resulted in fibrils containing both monomers, the fibrils were collected by centrifugation, resolubilized in 100% HFIP, and analyzed by ESI-MS (Fig. 4*D*). The resulting spectra contained peaks arising from hβ_2m and ΔN6 (masses 11,859 ± 1.19 and 11,136 ± 1.13 Da, respectively) with approximately equal intensity, suggesting that the protein monomers co-polymerize into fibrils with equal probability.

Finally, to confirm that both monomers are present in the same fibril, hβ_2m was labeled with TAMRA and ΔN6 with FITC under conditions that modify a single lysine on average. Fibril formation of each monomeric sample and the mixed sample was then allowed to proceed for 96 h at pH 6.2. The homo- and hetero-polymeric fibrils formed ("Experimental Procedures") were then compared using confocal fluorescence microscopy. The resulting images (15–20 per sample) and co-localization plots (Fig. 4, *E–H*) show that in the mixed sample both labeled monomers assemble into a single fibril containing approximately equal amounts of each protein precursor. These results provide further evidence that ΔN6 is able to convert hβ_2m into a conformation able to co-assemble with ΔN6 to form heteropolymeric fibrils.

Limited Proteolysis of Different Fibril Polymorphs—We next compared the fibril cores of the three different fibril types. Previous studies using limited proteolysis combined with mass spectrometry (23) have shown that the N-terminal 9 residues of hβ_2m fibrils formed at pH 2.5 are accessible to pepsin cleavage, implying the 90 remaining residues are part of the fibril core. A different fibril polymorph formed from the same protein at pH 3.6 (known as "worm-like" fibrils) possesses a less extensive core involving residues 40–74 (23). To determine the extent of the cores in ΔN6 homopolymeric fibrils and in heteropolymeric fibrils, cleavage with chymotrypsin or aspergillopepsin I was performed. The former enzyme cleaves predominantly at aromatic residues, with a reduced propensity to cleave at leucine and methionine. Its optimal activity occurs at pH 8 (41). Because hβ_2m fibrils formed at pH 2 dissociate at this pH, incubation with aspergillopepsin I was used to cleave hβ_2m fibrils at pH 2. Aspergillopepsin I has a propensity to cleave at basic amino acids and is catalytically active between pH 1 and 6 (42). As a consequence, this proteinase was also used to cleave ΔN6 fibrils and the mixed fibrils.

The cleavage products detected after digestion of ΔN6 fibrils with chymotrypsin or aspergillopepsin I are shown diagrammatically in Fig. 5. Cleavage of ΔN6 fibrils with both proteinases occurred close to the termini (Gln-8, Tyr-10, Leu-87, and Trp-95) (numbering according to the hβ_2m sequence), resulting in peptides encompassing amino acids 9–99, 11–95, 11–99, 7–87, and 7–95. No cleavage was observed between residues 10 and 87 despite the presence of many potential cleavage sites (potential chymotrypsin cleavage sites depicted by the *gray bar* in Fig. 5). The results suggest that in ΔN6 fibrils residues 12–86 form the core.

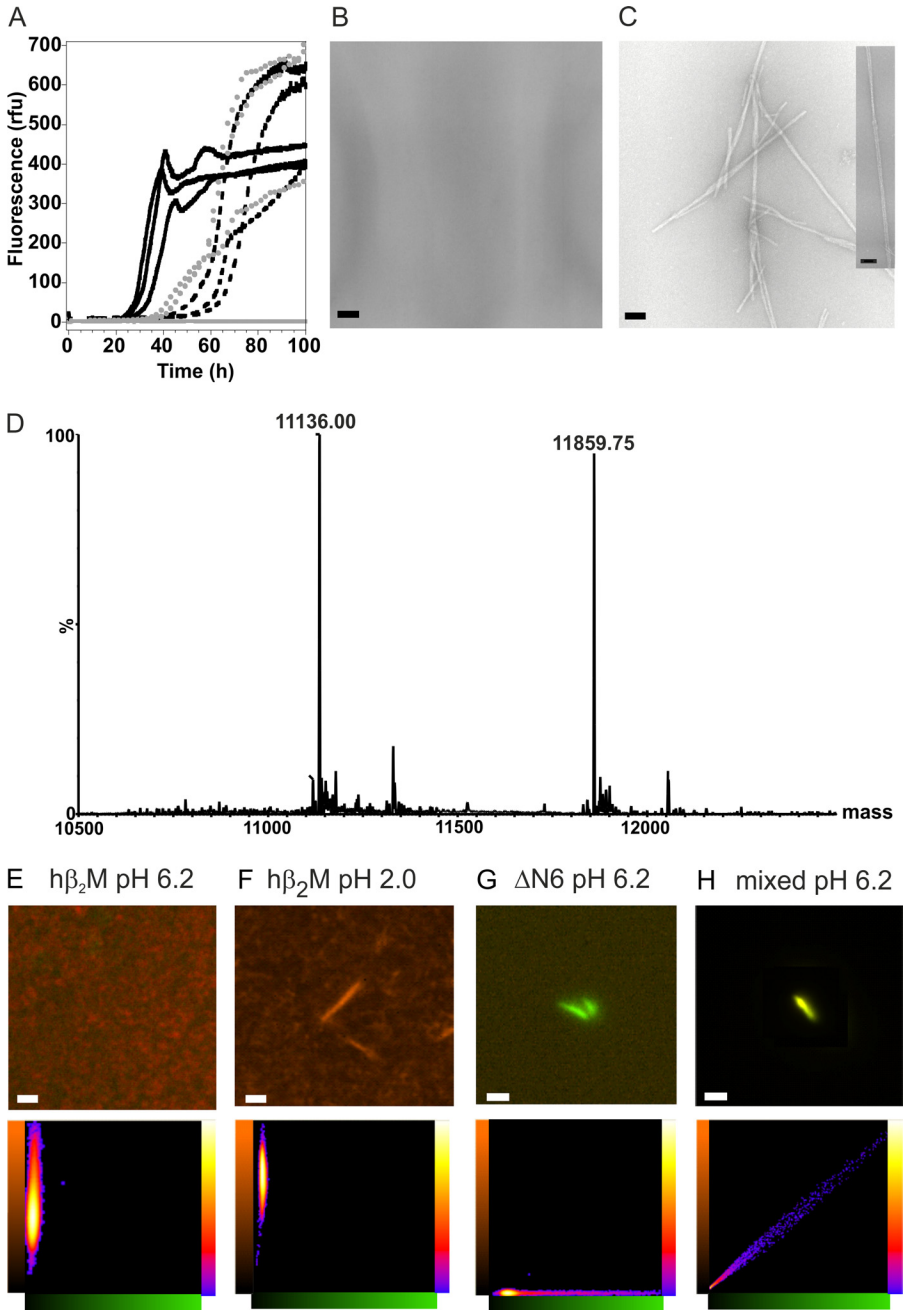

FIGURE 4. **Characterization of fibrils formed from mixtures of ΔN6 and hβ_2m at pH 6.2.** *A*, shown are ThT fluorescence traces of ΔN6 at 60 μM (*solid black*), 120 μM (*dashed black*), and a 60:60 μM mixture of ΔN6 and hβ_2m (*dashed gray*). Note hβ_2m incubated alone (60 and 120 μM) does not form fibrils under these conditions (*solid gray*). The kinetic traces of three different replicates are shown for each sample. Shown are negative stain EM images of the end point of incubation of hβ_2m alone (*B*) and the ΔN6:hβ_2m mixed fibril sample (the *inset* shows a single fibril; *C*) both at pH 6.2; *scale bars* are 100 nm. *rfu*, relative fluorescence units. *D*, shown is an ESI mass spectrum of depolymerized fibrils formed from a 1:1 (mol/mol) mixture of hβ_2m (11,859 Da) and ΔN6 (11,136 Da). *E*, shown are fluorescence microscopy images of TAMRA-labeled hβ_2m at pH 6.2 (no fibrils). *F*, shown are fibrils of TAMRA-hβ_2m formed at pH 2. FITC-labeled ΔN6 fibrils formed at pH 6.2 (*G*) and fibrils formed from a 1:1 (mol/mol) mixture of TAMRA-hβ_2m monomers and FITC-ΔN6 (*H*) are shown. The *yellow color* shows the superposition of red and green fluorescence. *Scale bar* = 5 μm. The scattergraphs depict co-localization plots of the contribution from the green (FITC fluorescence, *x* axis) and red (TAMRA fluorescence, *y* axis) channels for each pixel location. The y2 axis is the intensity of the signal. The images are 8 bit, thus the x and y axes are from 0–256 pixels.

For comparison, monomeric ΔN6 was also cleaved with chymotrypsin. Cleavage sites were observed at Tyr-26, Leu-40, Trp-60, Tyr-66, and Lys-75 consistent with the NMR structure of ΔN6 (25), which reveals these residues are located in surface-exposed loops. Accordingly, peptides 7–60, 27–60, 40–60, 61–99, 67–99, and 76–99 are identified using ESI-MS and ESI-MS/MS (Fig. 5).

The chymotrypsin or aspergillopepsin I cleavage patterns for β_2m/ΔN6 heteropolymeric fibrils (Fig. 5) revealed that the core of these fibrils resembles that of fibrils formed from ΔN6 alone. Cleavage sites were observed at residues Gln-8, Tyr-10, Leu-87, and Trp-95, resulting in peptides 9–99, 11–99, 0–87, and 0–95 respectively. The core of these heteropolymeric fibrils, thus, also involves residues 12–86. Cleavage of hβ_2m fibrils with

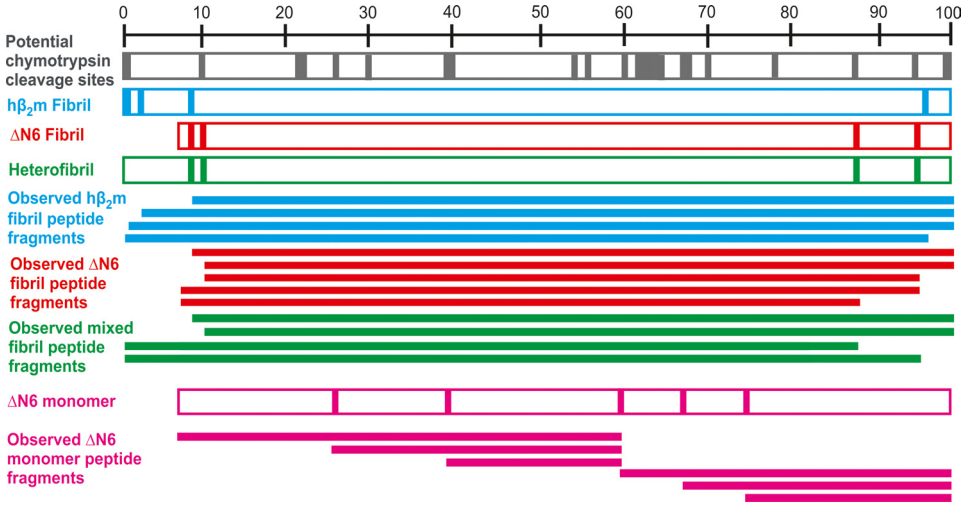

FIGURE 5. **Limited proteolysis of ΔN6 monomer, hβ_2m, and ΔN6 homopolymeric fibrils and heteropolymeric fibrils.** Limited proteolysis was performed using aspergillopepsin I at pH 6 and chymotrypsin at pH 8 (ΔN6 fibrils, mixed fibrils, and ΔN6 monomer) or aspergillopepsin I only at pH 2 (hβ_2m fibrils) at a 1:100 (w/w) proteinase:protein ratio, mapped using ESI-MS and ESI-MS/MS. Potential chymotrypsin cleavage sites are found throughout the sequence of hβ_2m (*gray bar*). Cleavage sites in the fibrils and ΔN6 monomer are shown using *vertical bars*. The *horizontal filled bars* represent the peptide fragments observed. Cleavage of ΔN6 monomers with chymotrypsin at pH 8 is also shown (*pink*).

aspergillopepsin I at pH 2.0 showed cleavages at Met-0, Gln-2, Gln-8, and Asp-96 (resulting in the peptides 1–99, 3–99, 9–99, and 0–96 (Fig. 5)), consistent with previous results suggesting a more extensive fibril core (residues 10–95) (23).

Spectroscopic Analysis of Homopolymeric and Heteropolymeric Fibrils—Having demonstrated the ability of ΔN6 and hβ_2m to assemble alone (at different pH) or together (at pH 6.2) into homopolymeric or heteropolymeric fibrils with similar fibril cores, we next sought to characterize the conformational properties of the different fibrils formed using spectroscopic analyses. FTIR spectroscopy is able to distinguish between amyloid fibrils and other β-sheet-containing structures. The cross-β architecture of amyloid results in an absorbance band at ~1620 cm^{-1}, whereas β-sheet structures in globular proteins absorb typically at around 1640 cm^{-1} (22).

To confirm that incubation of ΔN6 monomers at pH 6.2 results in fibrils with the characteristic properties of amyloid and to compare the underlying structures of the amyloid fibrils formed from hβ_2m at pH 2.0, ΔN6 at pH 6.2, and the 1:1 mixture of hβ_2m:ΔN6 at pH 6.2, each of the fibril samples was analyzed using FTIR (Fig. 6*A*). All three fibril types give rise to a maximum absorbance band at 1620 cm^{-1}, typical of amyloid. Indeed, the FTIR spectrum of the heteropolymeric fibril sample is indistinguishable from that of ΔN6 fibrils, whereas the hβ_2m fibrils give rise to an additional band at ~1650 cm^{-1} that has been observed previously for these fibrils (22). By contrast, monomeric ΔN6 gives rise to an absorbance maximum at ~1640 cm^{-1}, typical of that expected for β-sheet structure within globular proteins, whereas hβ_2m monomers at pH 2.0 show an absorbance maximum at ~1650 cm^{-1}, typical of unfolded polypeptide chains (43).

The anti-fibril antibody (IgM) WO1 binds to an epitope found in many amyloid fibrils and is a useful tool for confirming that fibrils have an amyloid conformation (35). All three fibril types were dotted onto nitrocellulose membranes and incubated with the WO1 anti-fibrillar antibody using an anti-β_2m antibody as a control. In all three fibril types a strong positive

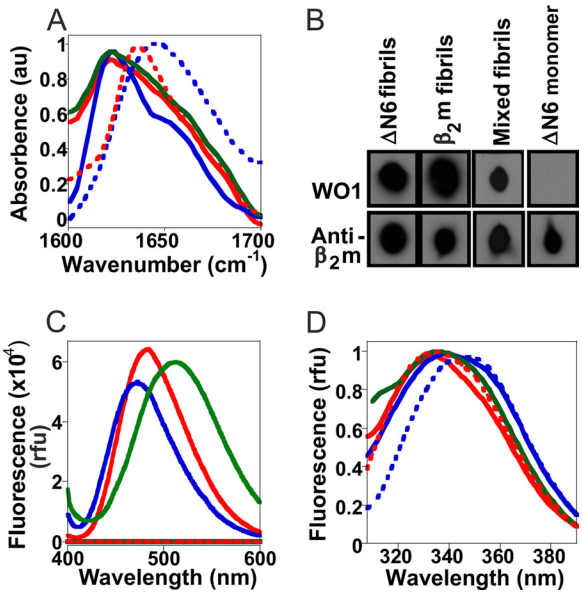

FIGURE 6. **Spectroscopic analysis of the fibrils formed from ΔN6, hβ_2m, and a mixture of the two monomers.** *A*, shown are FTIR absorbance spectra of hβ_2m monomer at pH 2 (*blue*) and ΔN6 (*red*) monomer at pH 6.2 (*dotted lines*) and fibrils formed from hβ_2m pH 2 (*blue solid line*), ΔN6 at pH 6.2 (*red solid line*) and a 1:1 mixture of ΔN6:hβ_2m at pH 6.2 (*green*). For clarity the spectrum of ΔN6 fibrils has been vertically offset. Its spectrum is otherwise very similar to that of the heteropolymeric fibrils. *au*, normalized absorbence units. *B*, dot blots of different samples incubated with the antibody WO1 and a polyclonal anti-β_2m antibody are shown. *C*, shown are fluorescence emission spectra of ANS in the presence of fibrils formed from ΔN6 (*red*), hβ_2m (*blue*), and the mixed fibrils (*green*). Spectra of monomeric ΔN6 and hβ_2m are also shown at ~0 relative fluorescence units (*rfu*). *D*, shown are intrinsic fluorescence emission spectra of ΔN6 monomer at pH 6.2 (*red dotted line*) and hβ_2m monomer at pH 2 (*blue dotted line*) and hβ_2m fibrils (*blue solid line*), ΔN6 fibrils (*red solid line*) and the mixed fibrils (*green*).

reactivity resulted from incubation with WO1 (Fig. 6*B*), consistent with the presence of cross-β structures. As expected, no binding of WO1 was observed to ΔN6 monomers.

The organization of side chains in the three fibril types was then probed using binding of the dye ANS as an indication of surface-exposed hydrophobicity (Fig. 6*C*) and the fluorescence

emission of the tryptophan residues to indicate differences in the environment of the two tryptophan residues in the three fibril types (Fig. 6*D*). Interestingly, incubation of each fibril type with ANS resulted in different fluorescence emission spectra, suggesting differences in surface hydrophobicity. The fluorescence emission λ_{max} values for ANS were 513, 485, and 474 nm for heteropolymeric fibrils, ΔN6 fibrils, and hβ_2m fibrils, respectively, compared with 544 nm for free ANS. Note that the λ_{max} of ANS does not change between pH 2 and 6.2, although the intensity of the emission is pH-dependent (data not shown).

hβ_2m and ΔN6 contain two tryptophan residues. Trp-60 is solvent-exposed, whereas Trp-95 is buried from solvent in both folded proteins (25). By contrast, Trp-95 is solvent-exposed in the fibrils formed from hβ_2m at pH 2 (44). At pH 6.2 the fluorescence emission spectrum of monomeric ΔN6 has a $\lambda_{max} \sim$ 335 nm, similar to that of hβ_2m at neutral pH (44), suggesting that the environments for the two tryptophan residues are similar to those of native hβ_2m (25). By contrast, the spectrum of monomeric hβ_2m at pH 2.0 has a λ_{max} at 345 nm, consistent with unfolding of the protein at this pH. The tryptophan fluorescence emission spectra of the proteins in the three fibril types differ significantly; although a blue shift in the fluorescence maximum was observed for all three fibril samples compared with their monomeric precursors, the magnitude of this shift differs significantly for the different samples (ΔN6 fibrils λ_{max} = 330 nm; hβ_2m fibrils at pH 2 λ_{max} = 340 nm; heteropolymeric fibril sample λ_{max} = 336 nm). These data indicate that the packing of the indole rings of Trp-60 and/or Trp-95 differs in the three fibril types, consistent with the results obtained using ANS fluorescence described above.

Fibril Polymorphs Have Different Stability—The studies described above have shown that the heteropolymeric fibrils composed of hβ_2m and ΔN6 form a unique polymorph with properties distinct from both of their homopolymeric counterparts. To determine how the structural differences observed for the three fibril types influence their stability, each sample was titrated with GuHCl, and the extent of denaturation was determined by quantifying the amount of soluble material released after incubation of each sample for 1.5 h at each concentration of denaturant ("Experimental Procedures"). Stability was determined at the pH at which the fibrils were initially formed at (pH 2 for hβ_2m fibrils and pH 6.2 for ΔN6 and the heteropolymeric fibrils). The results of these experiments (Fig. 7) show that the ΔN6 fibrils are significantly less stable than the fibrils formed from hβ_2m, with an apparent denaturation midpoint of 2.2 M GuHCl compared with 4.2 M for hβ_2m fibrils. The heteropolymeric fibril sample is less stable than both of its homopolymeric counterparts, with an apparent midpoint for denaturation of 1.5 M GuHCl. Even in the absence of GuHCl, significant soluble material was present in the supernatant of the mixed fibrils after ultracentrifugation, suggesting that the critical concentration for polymerization is increased for this combination of monomer precursors compared with hβ_2m or ΔN6 assembly alone.

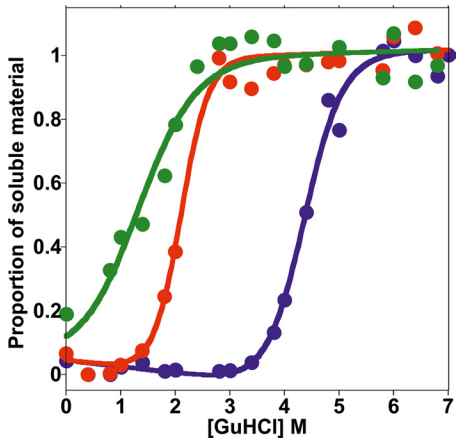

FIGURE 7. **Thermodynamic stability of fibrils formed from ΔN6 (*red*), hβ_2m (*blue*), and heteropolymeric fibrils (*green*).** The release of soluble material was measured using absorbance at 280 nm after incubation in GuHCl for 1.5 h. The results are presented as the proportion of soluble material by dividing the concentration of the soluble monomer by the total starting monomer concentration. The fit is to guide the eye.

DISCUSSION

Here we have investigated the effects of a naturally occurring N-terminal truncation of β_2m on the thermodynamic and structural properties of amyloid fibrils formed from this variant alone or from a 1:1 mixture of hβ_2m and ΔN6 monomers. Despite subtle differences in the structures of ΔN6 and hβ_2m monomers at pH 6.2, these two proteins possess fundamentally different abilities to form amyloid fibrils at this pH (25). We show here that the two proteins are able to co-polymerize to form amyloid fibrils that have unique structural and thermodynamic properties.

Fig. 8 depicts three possible schemes for how co-polymerization of hβ_2m and ΔN6 may occur. The central path begins with a collision between monomeric hβ_2m and ΔN6, whereupon hβ_2m undergoes a conformational conversion to an amyloid-competent state (25). This is thought to occur by the displacement of the A-strand from the native β-sandwich structure of hβ_2m (25), leading to isomerization of cis Pro-32 to trans, and further partial unfolding of hβ_2m. The equal incorporation of hβ_2m and ΔN6 monomers into heteropolymers, as shown here by mass spectrometry and confocal microscopy, are consistent with such a scheme.

Another possibility, shown in the *top scheme* in Fig. 8 is that ΔN6 forms a homopolymeric oligomer followed by an interaction with hβ_2m, from which the heteropolymeric fibrils form. These heteropolymeric oligomers may also form from an initial ΔN6:hβ_2m dimer, with the two pathways in a dynamic equilibrium. The final pathway, depicted as the *lower scheme* in Fig. 8, is that ΔN6 forms homopolymeric fibrils first, which then seed elongation with monomeric hβ_2m. A seeding mechanism for the system described here, although possible (45), is unlikely for two reasons. First, the ThT kinetics show that the presence of hβ_2m extends the lag phase of ΔN6 fibril formation compared with the same concentration of ΔN6 incubated alone, suggesting that an interaction occurs between hβ_2m and ΔN6 before fibrils are formed. Second, the confocal images of the fibrils formed from mixing ΔN6 and hβ_2m show no evidence of a seeded-elongation reaction such as that observed for extension of hβ_2m at pH 2 (46) and in other systems (47). Overall, therefore, heteropolymerization is most likely to occur through monomer-monomer or monomer-oligomer interactions of

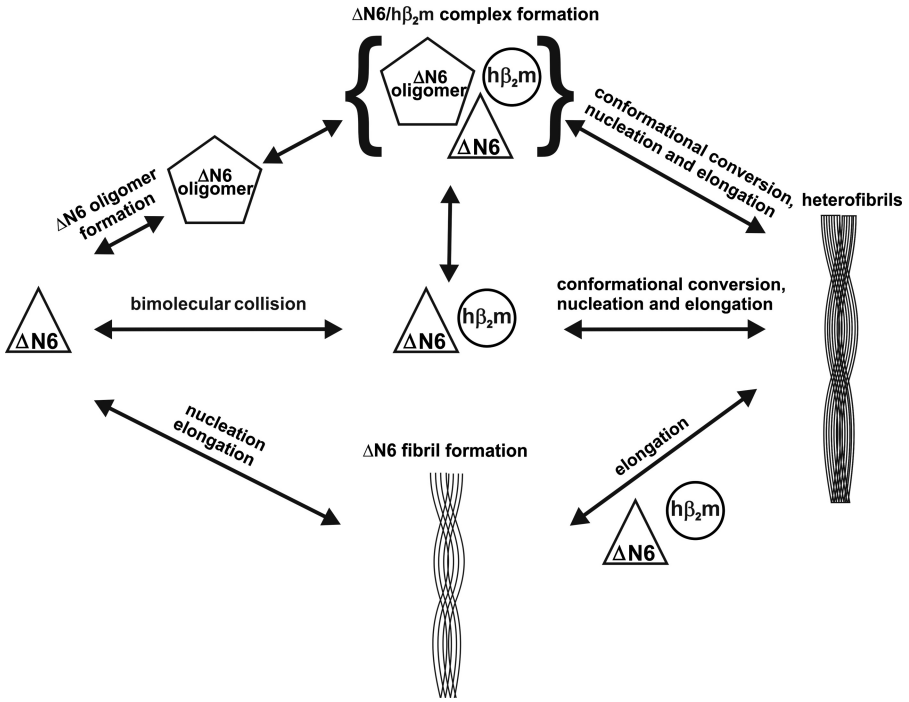

FIGURE 8. **Co-polymerization of hβ_2m and ΔN6 can occur by a variety of different possible mechanisms, involving oligomer formation, initial heterodimer formation, or cross-seeding.** See Discussion for details.

hβ_2m and ΔN6. As a consequence, sequence truncation not only results in the ability of hβ_2m to form amyloid fibrils at neutral pH but also results in the formation of a heteropolymeric fibril with unique properties.

Amyloid Polymorphism Revealed through the Co-polymerization of β_2m—Different packing of side chains in the hβ_2m, ΔN6, and the heteropolymeric fibrils, indicated by their MAS NMR spectra, ANS binding, and tryptophan fluorescence spectra, results in a pronounced difference in the stability of the fibrils formed. Polymorphism has been previously categorized based on structure (48); however, here we portray an additional form of polymorphism, termed here "stability polymorphism," in which co-polymerization of related fibril precursors leads to fibrils with unique structural and thermodynamic signatures. Whether stability polymorphism affects the biological response to fibrils requires further study. Given that amyloid plaques *in vivo* have been shown to be reservoirs of toxic oligomers (49), differences in amyloid stability and, therefore, the rate of depolymerization into harmful species may indeed result in differential effects of fibrils on cell toxicity.

Polymorphism and co-polymerization of proteins are intimately linked, with polypeptide heterogeneity giving rise to an array of potential changes in amyloid structure and/or stability. Fibrils composed of multiple species can arise through co-polymerization of two pools of monomer as shown here as well as through cross-seeding, in which existing fibrils (seeds) of one species catalyze fibril formation of monomers of a different sequence. This "dock and lock mechanism" occurs when a fully solvated monomer weakly binds to the peptides in the fibril and adopts their conformation (50, 51). When seeds are present, they can also have the effect of templating their structure onto the monomer pool, resulting in a structurally different seeded fibril to *de novo* fibrils formed by their unseeded counterparts (52). Some amyloid fibrils are also capable of accommodating peptides with mismatched sequences, enabling conformational switching during the cross-seeding reaction that results in fibrils of a new structure (53). However, there are limits to cross-seeding; as the sequence identity between the seed and the monomer decreases, the efficiency of the seeding reaction is reduced (14). Such events give rise to the species barrier in which a protein from one species is unable to seed the same protein from a different species, such as observed for prions (54), hβ_2m, and murine β_2m (25) as well as other protein species (55).

Co-polymerization; a Common Feature of Amyloid Assembly—Co-polymerization of different protein precursors may be a common phenomenon in amyloid disease. *In vivo*, many amyloid deposits are heterogeneous in composition, containing monomers with variations in protein length (truncations), sequence (mutations), composition (*e.g.* the ratio of Aβ40:Aβ42), post-translational modifications, and the presence of amyloid-associated co-factors (for review, see Ref. 48). In the system described here we demonstrated the co-polymerization of β_2m and its truncated counterpart ΔN6. This has relevance to the disease dialysis-related amyloidosis, as ~30% of the protein found in amyloid plaques is ΔN6, with the remainder being predominantly hβ_2m (26). Whether co-polymerization of these proteins occurs during assembly or post-assembly by proteolysis of the hβ_2m homopolymer is not clear. Likewise in Alzheimer disease N-terminally truncated, pyroglutamated forms of amyloid-β-peptide co-polymerize with Aβ42 at levels as low as 5% mol/mol, resulting in oligomers that are more toxic than either protein oligomerizing alone (56). Additionally the ratio of Aβ40:42 has been shown to be critical in determining toxicity and the area of amyloid deposition in Alzheimer disease (for review, see Ref. 48). Although Aβ42 was thought to be

the predominant toxic species in Alzheimer disease, there is now evidence that Aβ43 can accelerate amyloid-β pathology, as Aβ43 has a higher propensity to aggregate and is more neurotoxic than Aβ42 (57). Such species are capable of co-polymerization, which presumably will result in an array of different oligomeric and fibrillar species with unique structural, thermodynamic, kinetic, and functional properties.

Inclusions of tau and α-synuclein are present in individuals with sporadic neurodegenerative disorders, and a two-step mechanism of initiation followed by propagation has been proposed to explain how these two proteins interact (58). Similarly an elegant study using immunogold labeling of transthyretin-derived peptides showed that various guest peptides can be randomly inserted into the growing fibril (59). Moreover the same study used insulin fibrils doped with transthyretin peptides and found that the kinetics of fibril formation of both species must be relatively evenly matched for co-polymerization to occur (59). Co-incubation of proteins can also result in suppression of fibril formation. In yeast the interactions between different prions through cross-seeding can promote or inhibit prion propagation (60). A conformationally constrained analog of (islet amyloid polypeptide), designed to be a mimic of the non-amyloidogenic IAPP conformation, has also been shown to be able to bind prefibrillar Aβ and heteroassociate to block and reverse Aβ self-assembly (61).

The structural and thermodynamic studies described here demonstrate that combining β_2m and ΔN6 monomers does not prevent fibril formation but in fact can enhance the ability of hβ_2m to form fibrils and extend the repertoire of polymorphs formed. We reveal here that the heteropolymers formed by co-polymerization of ΔN6 and hβ_2m have unique structural properties and a unique thermodynamic signature compared with their homopolymeric forms. How this is encoded by differences in structure will require further high resolution information, so that the thermodynamic differences can be rationalized in structural terms. Understanding this process further may also shed light on the fundamental molecular mechanisms of fibril formation and how the presence of heteropolymeric assemblies can affect the extent, rate, and biological consequences of amyloid deposition.

Acknowledgments—We thank David Brockwell and members of our research groups for helpful discussions and comments. We thank Geoff Platt for expressing and purifying the hβ_2m used in the MAS NMR, Ronald Wetzel for kindly providing the antibody WO1, James Ault for mass spectrometric analysis of the disulfide bond formation and the protein composition of the heteropolymeric fibrils, Theodoros Karamanos for help with solution NMR, Gareth Howell for help with the confocal microscopy, and Toral Jakhria and Kevin Tipping for advice on fluorescence labeling and for performing the dot blots.

REFERENCES

1. Querfurth, H. W., and LaFerla, F. M. (2010) Alzheimer's disease. *N. Engl. J. Med.* **362,** 329–344
2. Goedert, M. (2001) α-Synuclein and neurodegenerative diseases. *Nat. Rev. Neurosci.* **2,** 492–501
3. Westermark, P., Wernstedt, C., Wilander, E., Hayden, D. W., O'Brien, T. D., and Johnson, K. H. (1987) Amyloid fibrils in human insulinoma and islets of Langerhans of the diabetic cat are derived from a neuropeptide-like protein also present in normal islet cells. *Proc. Natl. Acad. Sci. U.S.A.* **84,** 3881–3885
4. Gejyo, F., Yamada, T., Odani, S., Nakagawa, Y., Arakawa, M., Kunitomo, T., Kataoka, H., Suzuki, M., Hirasawa, Y., and Shirahama, T. (1985) A new form of amyloid protein associated with chronic hemodialysis was identified as β2-microglobulin. *Biochem. Biophys. Res. Commun.* **129,** 701–706
5. Valleix, S., Gillmore, J. D., Bridoux, F., Mangione, P. P., Dogan, A., Nedelec, B., Boimard, M., Touchard, G., Goujon, J. M., Lacombe, C., Lozeron, P., Adams, D., Lacroix, C., Maisonobe, T., Planté-Bordeneuve, V., Vrana, J. A., Theis, J. D., Giorgetti, S., Porcari, R., Ricagno, S., Bolognesi, M., Stoppini, M., Delpech, M., Pepys, M. B., Hawkins, P. N., and Bellotti, V. (2012) Hereditary systemic amyloidosis due to D76N variant β2-microglobulin. *N. Engl. J. Med.* **366,** 2276–2283
6. Greenwald, J., and Riek, R. (2010) Biology of amyloid. Structure, function, and regulation. *Structure* **18,** 1244–1260
7. Lewandowski, J. R., van der Wel, P. C., Rigney, M., Grigorieff, N., and Griffin, R. G. (2011) Structural complexity of a composite amyloid fibril. *J. Am. Chem. Soc.* **133,** 14686–14698
8. Wasmer, C., Schütz, A., Loquet, A., Buhtz, C., Greenwald, J., Riek, R., Böckmann, A., and Meier, B. H. (2009) The molecular organization of the fungal prion HET-s in its amyloid form. *J. Mol. Biol.* **394,** 119–127
9. Qiang, W., Yau, W. M., Luo, Y., Mattson, M. P., and Tycko, R. (2012) Antiparallel β-sheet architecture in Iowa-mutant β-amyloid fibrils. *Proc. Natl. Acad. Sci. U.S.A.* **109,** 4443–4448
10. Debelouchina, G. T., Platt, G. W., Bayro, M. J., Radford, S. E., and Griffin, R. G. (2010) Intermolecular alignment in β(2)-microglobulin amyloid fibrils. *J. Am. Chem. Soc.* **132,** 17077–17079
11. Goldschmidt, L., Teng, P. K., Riek, R., and Eisenberg, D. (2010) Identifying the amylome, proteins capable of forming amyloid-like fibrils. *Proc. Natl. Acad. Sci. U.S.A.* **107,** 3487–3492
12. Eichner, T., and Radford, S. E. (2011) A diversity of assembly mechanisms of a generic amyloid fold. *Mol. Cell* **43,** 8–18
13. Kelly, J. W. (1998) The alternative conformations of amyloidogenic proteins and their multi-step assembly pathways. *Curr. Opin. Struct. Biol.* **8,** 101–106
14. Krebs, M. R., Morozova-Roche, L. A., Daniel, K., Robinson, C. V., and Dobson, C. M. (2004) Observation of sequence specificity in the seeding of protein amyloid fibrils. *Protein Sci.* **13,** 1933–1938
15. Suzuki, N., Cheung, T. T., Cai, X. D., Odaka, A., Otvos, L., Jr., Eckman, C., Golde, T. E., and Younkin, S. G. (1994) An increased percentage of long amyloid β protein secreted by familial amyloid β protein precursor (β APP717) mutants. *Science* **264,** 1336–1340
16. Johan, K., Westermark, G., Engström, U., Gustavsson, A., Hultman, P., and Westermark, P. (1998) Acceleration of amyloid protein A amyloidosis by amyloid-like synthetic fibrils. *Proc. Natl. Acad. Sci. U.S.A.* **95,** 2558–2563
17. Isenman, D. E., Painter, R. H., and Dorrington, K. J. (1975) The structure and function of immunoglobulin domains. Studies with β2-microglobulin on the role of the intrachain disulfide bond. *Proc. Natl. Acad. Sci. U.S.A.* **72,** 548–552
18. Hodkinson, J. P., Ashcroft, A. E., and Radford, S. E. (2012) in *Non-fibrillar Amyloidogenic Protein Assemblies. Common Cytotoxins Underlying Degenerative Disease* (Rahimi, F., and Bitan, G. eds) pp. 377–406, Springer Science, The Netherlands
19. Yanagi, K., Sakurai, K., Yoshimura, Y., Konuma, T., Lee, Y. H., Sugase, K., Ikegami, T., Naiki, H., and Goto, Y. (2012) The monomer-seed interaction mechanism in the formation of the β2-microglobulin amyloid fibril clarified by solution NMR techniques. *J. Mol. Biol.* **422,** 390–402
20. Platt, G. W., McParland, V. J., Kalverda, A. P., Homans, S. W., and Radford, S. E. (2005) Dynamics in the unfolded state of β2-microglobulin studied by NMR. *J. Mol. Biol.* **346,** 279–294
21. Ladner, C. L., Chen, M., Smith, D. P., Platt, G. W., Radford, S. E., and Langen, R. (2010) Stacked sets of parallel, in-register β-strands of β2-microglobulin in amyloid fibrils revealed by site-directed spin labeling and chemical labeling. *J. Biol. Chem.* **285,** 17137–17147
22. Fabian, H., Gast, K., Laue, M., Misselwitz, R., Uchanska-Ziegler, B., Ziegler, A., and Naumann, D. (2008) Early stages of misfolding and association of β2-microglobulin. Insights from infrared spectroscopy and dynamic light scattering. *Biochemistry* **47,** 6895–6906

23. Myers, S. L., Thomson, N. H., Radford, S. E., and Ashcroft, A. E. (2006) Investigating the structural properties of amyloid-like fibrils formed *in vitro* from β2-microglobulin using limited proteolysis and electrospray ionization mass spectrometry. *Rapid Commun. Mass Spectrom.* **20,** 1628–1636
24. White, H. E., Hodgkinson, J. L., Jahn, T. R., Cohen-Krausz, S., Gosal, W. S., Müller, S., Orlova, E. V., Radford, S. E., and Saibil, H. R. (2009) Globular tetramers of β2-microglobulin assemble into elaborate amyloid fibrils. *J. Mol. Biol.* **389,** 48–57
25. Eichner, T., Kalverda, A. P., Thompson, G. S., Homans, S. W., and Radford, S. E. (2011) Conformational conversion during amyloid formation at atomic resolution. *Mol. Cell* **41,** 161–172
26. Bellotti, V., Stoppini, M., Mangione, P., Sunde, M., Robinson, C., Asti, L., Brancaccio, D., and Ferri, G. (1998) β2-microglobulin can be refolded into a native state from *ex vivo* amyloid fibrils. *Eur. J. Biochem.* **258,** 61–67
27. Yamaguchi, K., Katou, H., Hoshino, M., Hasegawa, K., Naiki, H., and Goto, Y. (2004) Core and heterogeneity of β2-microglobulin amyloid fibrils as revealed by H/D exchange. *J. Mol. Biol.* **338,** 559–571
28. Esposito, G., Michelutti, R., Verdone, G., Viglino, P., Hernández, H., Robinson, C. V., Amoresano, A., Dal Piaz, F., Monti, M., Pucci, P., Mangione, P., Stoppini, M., Merlini, G., Ferri, G., and Bellotti, V. (2000) Removal of the N-terminal hexapeptide from human β2-microglobulin facilitates protein aggregation and fibril formation. *Protein Sci.* **9,** 831–845
29. Hodkinson, J. P., Radford, S. E., and Ashcroft, A. E. (2012) The role of conformational flexibility in β2-microglobulin amyloid fibril formation at neutral pH. *Rapid Commun. Mass Spectrom.* **26,** 1783–1792
30. Ma, B., and Nussinov, R. (2003) Molecular dynamics simulations of the unfolding of β2-microglobulin and its variants. *Protein Eng.* **16,** 561–575
31. Eichner, T., and Radford, S. E. (2009) A generic mechanism of β2-microglobulin amyloid assembly at neutral pH involving a specific proline switch. *J. Mol. Biol.* **386,** 1312–1326
32. Bennett, A. E., Griffin, R. G., Ok, J. H., and Vega, S. (1992) Chemical shift correlation spectroscopy in rotating solids. Radio frequency driven dipolar recoupling and longitudinal exchange. *J. Chem. Phys.* **96,** 8624–8627
33. Bennett, A. E., Rienstra, C. M., Griffiths, J. M., Zhen, W. G., Lansbury, P. T., and Griffin, R. G. (1998) Homonuclear radio frequency-driven recoupling in rotating solids. *J. Chem. Phys.* **108,** 9463–9479
34. Bennett, A. E., Rienstra, C. M., Auger, M., Lakshmi, K. V., and Griffin, R. G. (1995) Heteronuclear decoupling in rotating solids. *J. Chem. Phys.* **103,** 6951–6958
35. O'Nuallain, B., and Wetzel, R. (2002) Conformational Abs recognizing a generic amyloid fibril epitope. *Proc. Natl. Acad. Sci. U.S.A.* **99,** 1485–1490
36. Xue, W. F., Hellewell, A. L., Gosal, W. S., Homans, S. W., Hewitt, E. W., and Radford, S. E. (2009) Fibril fragmentation enhances amyloid cytotoxicity. *J. Biol. Chem.* **284,** 34272–34282
37. Shammas, S. L., Knowles, T. P., Baldwin, A. J., Macphee, C. E., Welland, M. E., Dobson, C. M., and Devlin, G. L. (2011) Perturbation of the stability of amyloid fibrils through alteration of electrostatic interactions. *Biophys. J.* **100,** 2783–2791
38. Woods, L. A., Platt, G. W., Hellewell, A. L., Hewitt, E. W., Homans, S. W., Ashcroft, A. E., and Radford, S. E. (2011) Ligand binding to distinct states diverts aggregation of an amyloid-forming protein. *Nat. Chem. Biol.* **7,** 730–739
39. Liu, C., Sawaya, M. R., and Eisenberg, D. (2011) β2-microglobulin forms three-dimensional domain-swapped amyloid fibrils with disulfide linkages. *Nat. Struct. Mol. Biol.* **18,** 49–55
40. Iwadate, M., Asakura, T., and Williamson, M. P. (1999) C-α and C-β carbon-13 chemical shifts in proteins from an empirical database. *J. Biomol. NMR* **13,** 199–211
41. Appel, W. (1986) Chymotrypsin. Molecular and catalytic properties. *Clin. Biochem.* **19,** 317–322
42. Ichishima, E. (1970) Purification and mode of assay for acid proteinase of *Aspergillus saitoi*. *Methods Enzymol.* **19,** 397–406
43. Nilsson, M. R. (2004) Techniques to study amyloid fibril formation *in vitro*. *Methods* **34,** 151–160
44. Chatani, E., Ohnishi, R., Konuma, T., Sakurai, K., Naiki, H., and Goto, Y. (2010) Pre-steady-state kinetic analysis of the elongation of amyloid fibrils of β(2)-microglobulin with tryptophan mutagenesis. *J. Mol. Biol.* **400,** 1057–1066
45. Myers, S. L., Jones, S., Jahn, T. R., Morten, I. J., Tennent, G. A., Hewitt, E. W., and Radford, S. E. (2006) A systematic study of the effect of physiological factors on β2-microglobulin amyloid formation at neutral pH. *Biochemistry* **45,** 2311–2321
46. Hoshino, M., Katou, H., Hagihara, Y., Hasegawa, K., Naiki, H., and Goto, Y. (2002) Mapping the core of the β(2)-microglobulin amyloid fibril by H/D exchange. *Nat. Struct. Biol.* **9,** 332–336
47. Kodali, R., and Wetzel, R. (2007) Polymorphism in the intermediates and products of amyloid assembly. *Curr. Opin. Struct. Biol.* **17,** 48–57
48. Eisenberg, D., and Jucker, M. (2012) The amyloid state of proteins in human diseases. *Cell* **148,** 1188–1203
49. Koffie, R. M., Meyer-Luehmann, M., Hashimoto, T., Adams, K. W., Mielke, M. L., Garcia-Alloza, M., Micheva, K. D., Smith, S. J., Kim, M. L., Lee, V. M., Hyman, B. T., and Spires-Jones, T. L. (2009) Oligomeric amyloid β associates with postsynaptic densities and correlates with excitatory synapse loss near senile plaques. *Proc. Natl. Acad. Sci. U.S.A.* **106,** 4012–4017
50. Sawaya, M. R., Sambashivan, S., Nelson, R., Ivanova, M. I., Sievers, S. A., Apostol, M. I., Thompson, M. J., Balbirnie, M., Wiltzius, J. J., McFarlane, H. T., Madsen, A. Ø., Riekel, C., and Eisenberg, D. (2007) Atomic structures of amyloid cross-β spines reveal varied steric zippers. *Nature* **447,** 453–457
51. Nguyen, P. H., Li, M. S., Stock, G., Straub, J. E., and Thirumalai, D. (2007) Monomer adds to preformed structured oligomers of Aβ-peptides by a two-stage dock-lock mechanism. *Proc. Natl. Acad. Sci. U.S.A.* **104,** 111–116
52. Surmacz-Chwedoruk, W., Nieznańska, H., Wójcik, S., and Dzwolak, W. (2012) Cross-seeding of fibrils from two types of insulin induces new amyloid strains. *Biochemistry* **51,** 9460–9469
53. Makarava, N., Ostapchenko, V. G., Savtchenko, R., and Baskakov, I. V. (2009) Conformational switching within individual amyloid fibrils. *J. Biol. Chem.* **284,** 14386–14395
54. Kocisko, D. A., Priola, S. A., Raymond, G. J., Chesebro, B., Lansbury, P. T., Jr., and Caughey, B. (1995) Species specificity in the cell-free conversion of prion protein to protease-resistant forms. A model for the scrapie species barrier. *Proc. Natl. Acad. Sci. U.S.A.* **92,** 3923–3927
55. Ma, B., and Nussinov, R. (2012) Selective molecular recognition in amyloid growth and transmission and cross-species barriers. *J. Mol. Biol.* **421,** 172–184
56. Nussbaum, J. M., Schilling, S., Cynis, H., Silva, A., Swanson, E., Wangsanut, T., Tayler, K., Wiltgen, B., Hatami, A., Rönicke, R., Reymann, K., Hutter-Paier, B., Alexandru, A., Jagla, W., Graubner, S., Glabe, C. G., Demuth, H. U., and Bloom, G. S. (2012) Prion-like behaviour and tau-dependent cytotoxicity of pyroglutamylated amyloid-β. *Nature* **485,** 651–655
57. Saito, T., Suemoto, T., Brouwers, N., Sleegers, K., Funamoto, S., Mihira, N., Matsuba, Y., Yamada, K., Nilsson, P., Takano, J., Nishimura, M., Iwata, N., Van Broeckhoven, C., Ihara, Y., and Saido, T. C. (2011) Potent amyloidogenicity and pathogenicity of Aβ43. *Nat. Neurosci.* **14,** 1023–1032
58. Giasson, B. I., Forman, M. S., Higuchi, M., Golbe, L. I., Graves, C. L., Kotzbauer, P. T., Trojanowski, J. Q., and Lee, V. M. (2003) Initiation and synergistic fibrillization of tau and α-synuclein. *Science* **300,** 636–640
59. MacPhee, C. E., and Dobson, C. M. (2000) Formation of mixed fibrils demonstrates the generic nature and potential utility of amyloid nanostructures. *J. Am. Chem. Soc.* **122,** 12707–12713
60. Bradley, M. E., Edskes, H. K., Hong, J. Y., Wickner, R. B., and Liebman, S. W. (2002) Interactions among prions and prion "strains" in yeast. *Proc. Natl. Acad. Sci. U.S.A.* **99,** 16392–16399
61. Yan, L. M., Velkova, A., Tatarek-Nossol, M., Andreetto, E., and Kapurniotu, A. (2007) IAPP mimic blocks Aβ cytotoxic self-assembly. Cross-suppression of amyloid toxicity of Aβ and IAPP suggests a molecular link between Alzheimer's disease and type II diabetes. *Angew Chem. Int. Ed. Engl.* **46,** 1246–1252
62. Lapko, V. N., Smith, D. L., and Smith, J. B. (2000) Identification of an artifact in the mass spectrometry of proteins derivatized with iodoacetamide. *J. Mass Spectrom.* **35,** 572–575